Journal of Materials Chemistry A

Accepted Manuscript

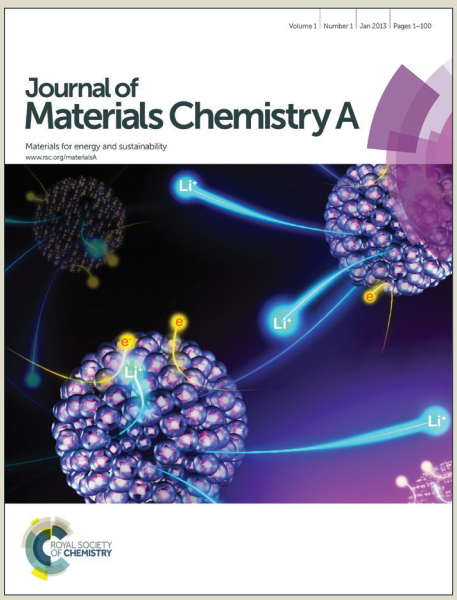

ROYAL SOCIETY OF CHEMISTRY

www.rsc.org/materialsA

Journal of Materials Chemistry A RSCPublishing

ARTICLE

Efficient solvent-assisted external treatment for planar heterojunction small-molecule organic solar cells

Cite this: DOI: 10.1039/xoxxoooooox

Received ooth January 2012,
Accepted ooth January 2012

DOI: 10.1039/xoxxoooooox

www.rsc.org/

Jinhyun Kim,[a] Ilsu Heo,[a] Dasom Park,[a] Sang Jung Ahn,[b] Sung-Yeon Jang,[*a] Sanggyu Yim[*a]

We developed a novel solvent-assisted treatment (SAT) technique to modify the nanomorphology of the planar heterojunction (PHJ) bilayer active layers (ZnPc/C_{60}) of organic photovoltaics (OPVs). The SAT technique uses organic solvent vapors under reduced pressures, which partially dissolves one component (the donor molecule, ZnPc, in this study) of PHJ layers prepared by vacuum deposition. Because of the partial mixing of the two layers, the PHJ layers develop a bulk heterojunction (BHJ)-like intermixed morphology. The performance of the resulting OPVs is considerably improved because of (i) the increased interfacial area of ZnPc/C_{60}, (ii) the healing of the intrinsic micropores within the active layers, which originate from the deposition process, and (iii) enhanced light absorption due to the rearrangement of the ZnPc molecules. After the SAT, the power conversion efficiency (PCE) of the OPVs improved more than three-fold (2.58%), with an open-circuit voltage (V_{OC}) of 0.61 V, a short-circuit current (J_{SC}) of 7.50 mA·cm^{-2}, and a fill factor (FF) of 0.56, as compared to that of the as-prepared PHJ-OPVs (PCE = 0.83%, with V_{OC} = 0.38 V, J_{SC} = 5.3 mA·cm^{-2}, and FF = 0.42). Our unique SAT technique provides an alternative route for controlling the nanomorphology of organic thin films by vacuum deposition, which may be very difficult to achieve using more conventional methods.

Introduction

Organic photovoltaic cells (OPV) have been extensively studied as promising candidates for next-generation solar cells because of their lower materials cost and applicability to flexible energy devices. Especially, active materials based on small molecules in OPV cells are attracting growing attention due to their high stability, easy purification, well-defined molecular structure and easy control of film growth.[1-4] Development of organic semiconducting materials has continuously increased the power conversion efficiency (PCE) of OPVs, reaching as high as ~10% while still possessing the potential for further improvement by designing new chemical structures.[5] In addition to materials development, manipulation of the interfacial nanomorphology within active layers, typically consisting of p-type and n-type semiconductors (also called donors and acceptors), is another crucial factor for optimizing the photon-to-electron conversion of OPVs.[6,7] Controlled nanomorphology in a way that offers a large contact area between donors and acceptors and the continuity of each domain can facilitate separation of the charges from excitons and the transport of the resulting charges to the collecting electrodes. The short exciton diffusion length in organic semiconductors limits the efficiency of charge separation before recombination, thus underscoring the importance of the nanomorphology.[8-10] Donor/acceptor (D/A) bulk heterojunction (BHJ)-structured active layers prepared by codeposition or homogeneous blending provide larger interface areas as compared to planar heterojunction (PHJ or bilayer structures) active layers, resulting in enhanced PCE.[11] However, excessive D/A phase separation can cause charge-carrier traps at the cul-de-sacs, hampering further increases in the device performance. Thus, appropriate phase segregation is an important issue.[12,13] In order to obtain preferential nanomorphology, interdigitated nanostructures of donors and acceptors have been proposed as offering enhanced interfaces for efficient exciton dissociation and charge transport simultaneously.[14,15] Various strategies for independently controlling the D/A phases, including nanoimprinting,[16-18] organic vapor phase deposition (OVPD),[12,13] and glancing-angle deposition (GLAD),[19-21] have been applied to fabricating these interdigitated nanostructures. Among these techniques, solvent-assisted treatment (SAT) using liquid drops,[22] vapor spray,[23] and saturated vapors[24] has recently attracted much attention as an emerging strategy because it provides a simple and fast process without the need for a sophisticated apparatus. Using this SAT method, nanopillars with diameters of 35–50 nm, which correspond to the exciton diffusion lengths of organic semiconductors, including phthalocyanine (Pc) films,[25-27] were successfully fabricated. Deposition of subsequent acceptor materials onto these donor nanopillars could lead to the formation of interdigitated D/A nanostructures. However, the fabrication of D/A interdigitated structures by this method can often yield poor interfaces containing undesirable voids, resulting in lower cell performance.

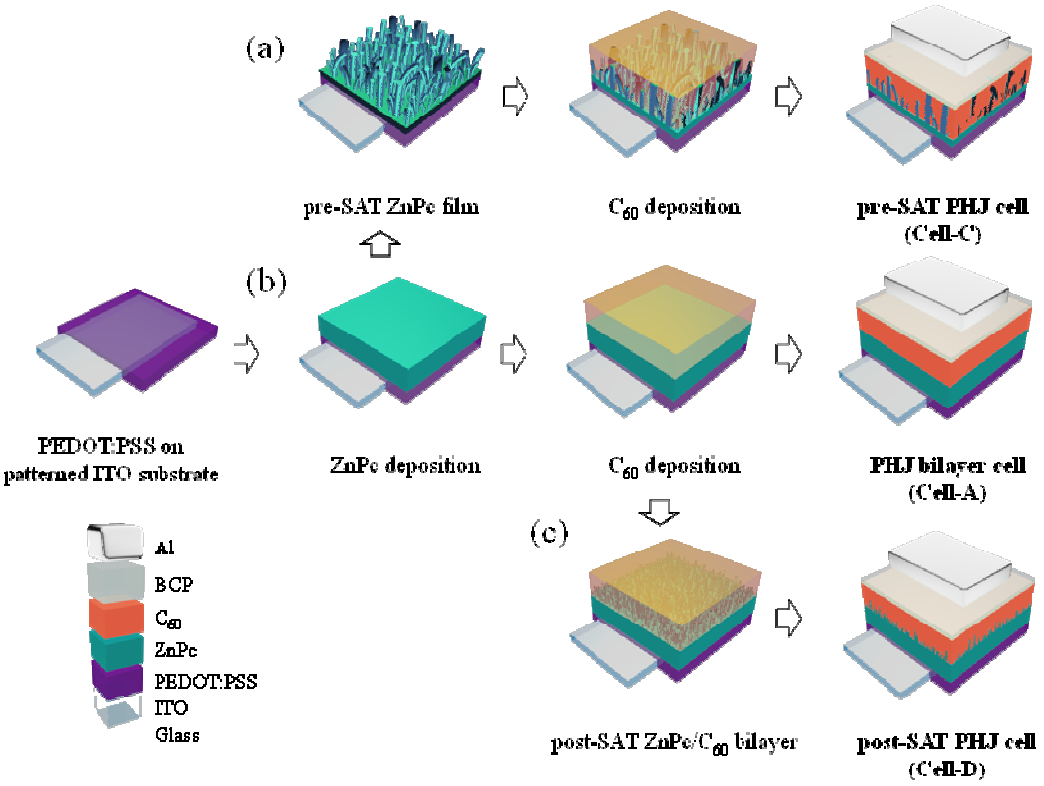

Figure 1 Schematic illustration of the structure of OPVs and the fabrication process of ZnPc/C_{60} active layers used in this study: (a) pre-SAT PHJ cell (Cell-C), (b) conventional PHJ bilayer cell (Cell-A), and (c) post-SAT PHJ cell (Cell-D). The BHJ cell (Cell-B) was fabricated using a conventional codeposition method as described in the experimental section

In this study, a novel SAT method for manipulating the nanomorphology of small molecules in the active layers of OPVs prepared by a vacuum process was developed. Zinc phthalocyanine (ZnPc) and C_{60} were used as the p-type (donor) and n-type (acceptor) semiconductors, respectively. Organic solvent vapors were then introduced under controlled pressure in order to rearrange the D/A interfaces of the initially formed PHJ bilayer to yield intermixed BHJ-like layers. The evolution in the nanomorphology of the active layers and the performance enhancement of the corresponding OPVs are discussed. Use of this SAT method on the ZnPc/C_{60} PHJ bilayer cells provided improved D/A contact with a higher interfacial area. The cell performance was also dramatically improved, showing a more than three-fold increase in PCE, low series resistance, and high shunt resistance, with a significantly higher open-circuit voltage (V_{OC} = 0.61 V) as compared to the untreated PHJ bilayer cells.

Results and discussion

The OPVs were fabricated by a conventional vacuum deposition method using ZnPc/C_{60} as the active materials. The active layers were prepared by four different routes, resulting in a i) conventional PHJ bilayer cell (Cell-A), ii) BHJ cell (Cell-B), iii) pre-SAT PHJ cell (Cell-C), and iv) post-SAT PHJ cell (Cell-D). A schematic illustration of the preparation procedure and structures for the four types of OPVs are shown in Figure 1. The current density–voltage (J–V) curves of these cells are shown in Figure 2, and the resulting cell characteristics are summarized in Table 1. The PCE of Cell-A, which contained an as-prepared PHJ bilayer as the active layer, was 0.83%, with a V_{OC} of 0.38 V, a short-circuit current density (J_{SC}) of

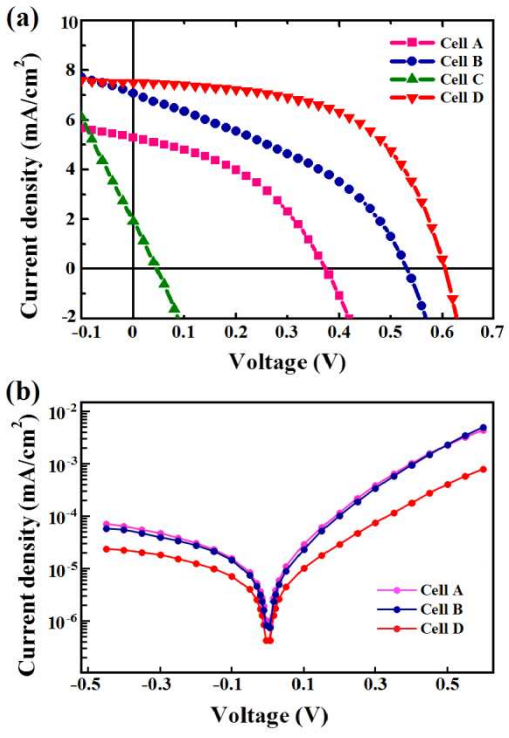

Figure 2 J–V characteristics of OPVs fabricated using various types of ZnPc/C_{60} layers measured at (a) AM 1.5G one sun illumination and (b) in the dark.

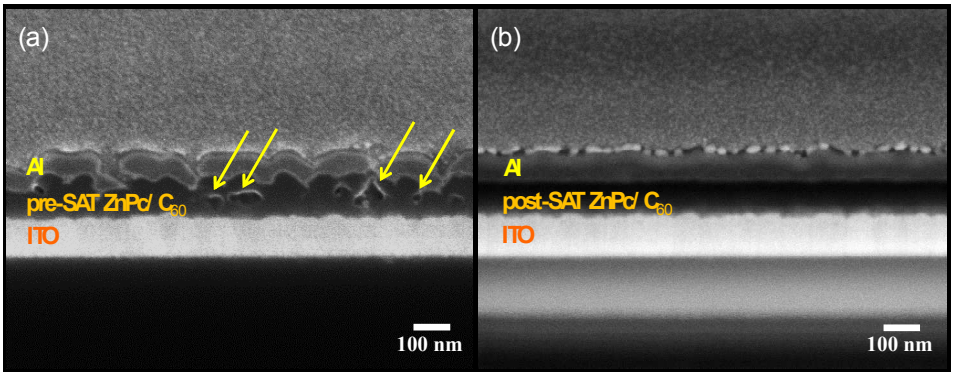

Figure 3 FE-SEM images of ZnPc/C_{60} active layers (a) pre-SAT (Cell-C) and (b) post-SAT (Cell-D). The yellow arrows in (a) indicate voids within the active layer.

5.3 mA·cm^{-2}, and a fill factor (FF) of 0.42. The relatively small D/A interfacial area of the bilayer structure limited further enhancement of J_{SC} and PCE. In the BHJ cell (Cell-B), in which the donors and acceptors were codeposited, the J_{SC} was improved to 7.07 mA·cm^{-2}, with a PCE of 1.45%. The enhanced interfacial area was responsible for the higher J_{SC} values as compared to the PHJ bilayer cells (Cell-A). However, additional optimization of the nanomorphology of the active layers such that charge carrier traps can be reduced needs to be addressed in order to further enhance other cell parameters such as FF and V_{OC}.

To obtain the desired interdigitated nanomorphology, which is known to result in efficient charge transport, we fabricated the active layers by depositing C_{60} on preformed ZnPc nanopillars.[23] The average diameters of the nanopillars were 35–42 nm (Figure S2 in Supporting Information, SI). The deposition of C_{60} on this ZnPc nanopillar layer was expected to form an interdigitated D/A structure capable of enhancing the cell performance. However, the PCE of this nanopillar-based interdigitated bilayer cell (Cell-C) was only ~0.02%. All other cell parameters, V_{OC} (0.05 V), J_{SC} (1.8 mA·cm^{-2}), and FF (0.26), were also quite low. We attributed these results to the fact that D/A interdigitation was not effectively formed because complete filling of the nanoscale spaces beneath the donor nanopillars with impinging acceptor molecules is very difficult [21,28]. Shadowing due to clogging of the pore entrances resulted in the formation of voids within the active layer, as clearly observed in the cross-sectional field-emission scanning electron microscopy (FE-SEM) images in Figure 3a. Apparently, the voids (indicated by arrows in Figure 3a) led to a significant increase in the series resistance (R_S) of the films, thus reducing the cell performance. In addition, the subsequent metal electrode (Al) deposition on top of the rough organic layer formed a very rough Al layer, which would cause resistive contact and irregular transport of charge carriers.

In order to construct a nanomorphology with an enhanced, void-free D/A interfacial area within the active layers, we applied the SAT after formation of the ZnPc/C_{60} bilayers (denoted as post-SAT, Cell-D). The changes in nanomorphology of organic active layers by similar SAT methods have been studied in polymer-based solar cells.[29-31] Application of a liquid or vapors of good or marginal solvents on bilayer or BHJ polymer films could alter the nanomorphology of these layers. Lee et al. reported the nanoscale intermixing of polymeric donors and acceptors by the spin coating of an acceptor solution in which the solvent is orthogonal to the donor film.[29] Our group also achieved a favorable nanomorphology by reorganization of polymer BHJ films using an appropriate amount of good solvent.[31,32] These reports demonstrate the enhancement of cell performance by effectively manipulating the nanomorphology of active layers using various SAT methods.[31,32] Motivated by these previous results, we attempted the reorganization of the nanomorphology of organic active layers using the SAT method. The SAT was performed in a separate solvent treatment chamber attached to the ultrahigh-vacuum (UHV) organic molecular beam deposition (OMBD) system (Figure S1). The chamber was saturated with acetone vapors introduced from an external liquid-containing cylinder. The pressure during the SAT was ~24 Torr (3.2 kPa). After the SAT, the sample was transferred back to the OMBD chamber and dried at 100°C for 1 h under ultrahigh vacuum, 2 × 10^{-8} Torr (2.67 μPa), to remove residual solvent before deposition of the Al electrode to form Cell-D.

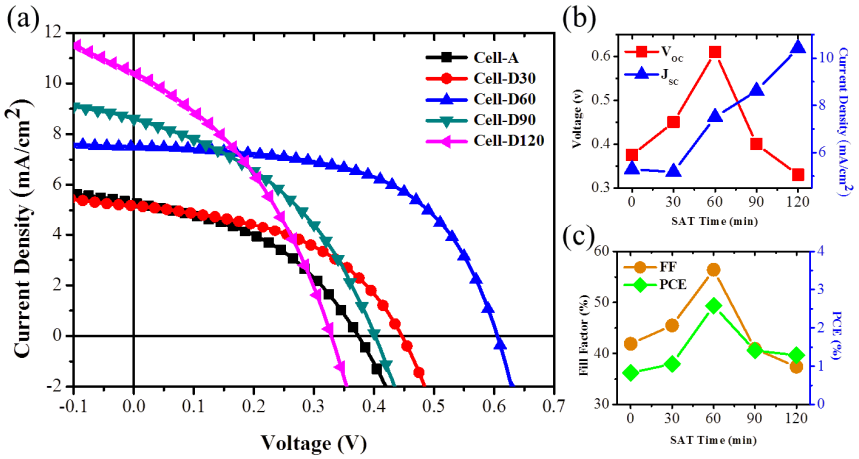

Figure 4 Characteristics of OPVs containing ZnPc/C_{60} layers: (a) *J–V* characteristics. The numbers after the cell labels indicate the SAT duration in minutes. Cell-A has the as-deposited ZnPc/C_{60} layers (0 min of SAT). (b) V_{OC} and J_{SC}. (c) FF and PCE. The *J–V* curves were measured at AM 1.5G one sun illumination.

Table 1 Performance of OPVs containing various ZnPc/C_{60} layers

Cell type	V_{OC} (V)	J_{SC} (mA·cm^{-2})	FF	PCE (%)
Cell-A	0.375	5.29	0.419	0.83
Cell-B	0.535	7.07	0.384	1.45
Cell-C	0.050	1.76	0.256	0.02
Cell-D	0.610	7.50	0.564	2.58

The cross-sectional FE-SEM image of the active layers after the SAT showed well-stacked, planar layers with an absence of voids (Figure 3b). Although any recognizable difference was not observed as compared to the as-deposited bilayers (Figure S3), the performance of the resulting OPVs was significantly enhanced after the SAT. The PCE of Cell-D was 2.58% (V_{OC} = 0.61 V, J_{SC} = 7.50 mA·cm^{-2}, FF = 0.56), which is 3.1 times higher than that of Cell-A, as summarized in Table 1.

The performance of Cell-D was also strongly influenced by the duration of the SAT. As shown in the *J*–*V* curves and the analyzed parameters of Cell-D for a range of SAT times (Figure 4a and Table 2), the performance was improved after 30 min of SAT (Cell-D30), nearly optimized after 60 min of SAT (Cell-D60), and then decreased continuously as the SAT time increased (Cell-D90 and Cell-D120). Interestingly, the J_{SC} values increased continuously with increasing SAT time, whereas the V_{OC} values reached a maximum in Cell-D60. The effects of SAT on the active layers were further investigated using optical analysis techniques. Figure 5 (right panel) exhibits the photoluminescence (PL) results for Cell-D over a range of SAT times. Because the PL of organic semiconductors occurs when the electron–hole pairs are relaxed by irradiative recombination, the PL intensity of the active layers can reveal the exciton dissociation efficiency at a D/A interface.[31] Also, because the PL of our active layers was quenched by the photo-induced charge transfer from ZnPc to C_{60}, the degree of PL quenching can indicate the efficiency of the charge dissociation. The as-deposited layers (Cell-A) exhibited relatively high PL intensity, indicating inefficient exciton dissociation due to a reduced D/A interfacial area. After SAT, the PL intensity decreased significantly, and it was reduced almost completely after 120 min. The inset graph in the right panel of Figure 5 shows the variation of PL intensity as a function of SAT time at λ = 1082 nm, which is the maximum emission wavelength of ZnPc thin films.[33] This result implies that the D/A contact areas increased as the duration of the SAT increased, which could induce improved charge separation. This result is consistent with the trend in the increase in the J_{SC} values (Figure 4 and Table 2). We attributed the increased D/A contact area to the intermixing of ZnPc and C_{60}. Because C_{60} is barely soluble in acetone, the soluble ZnPc is responsible for diffusion among the C_{60} molecules, thus forming enlarged interfaces. The remixing of the active materials and the change of nanomorphology (or D/A contact area) were also confirmed by TEM-mapping for Zn atoms (Figure S4). Note that the performance of Cell-D drastically decreased after 60 min of post-SAT, although the D/A interfacial area further increased. This is attributed to the fractional loss of domain continuity and the partial de-wetting of the thin active films by excessive SAT, as observed in our previous reports.[34]

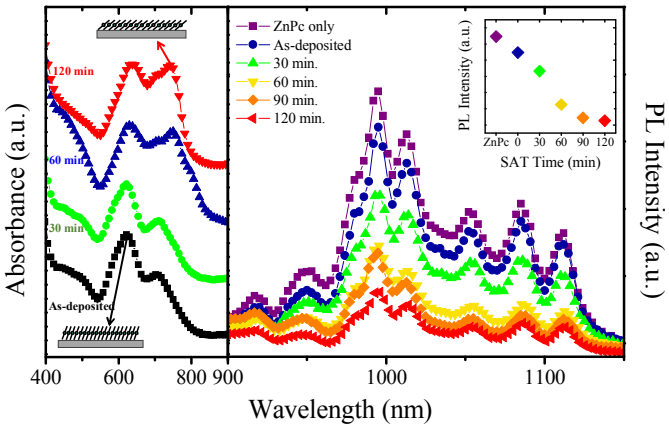

Figure 5 The UV-vis spectra (left panel) and PL intensity (right panel) of ZnPc/C_{60} layers subjected to SAT of various durations. The inset of the right panel shows the change in the PL intensity of the ZnPc/C_{60} layers as a function of SAT duration.

The SAT process also resulted in an alteration in the light-absorption properties of the active layers. The left panel of Figure 5 shows the electronic absorption (EA) spectra recorded for the active layers as a function of SAT duration. The EA spectrum of the as-deposited active layer exhibits characteristic α-phase ZnPc.[35] This absorption band is known as the superposition of three Q-bands of Pc films,[35] *i.e.*, Q_S, Q_L, and Q_M sub-bands, which are attributed to H-aggregates, J-aggregates, and medium transition aggregates, respectively. As shown in Figure 5 (left panel), a gradual change in the relative intensities of the sub-bands was observed as the SAT proceeded. The intensity of the Q_S band centered at 623 nm gradually decreased and that of the Q_L band centered at 747 nm increased. An especially large change was observed for Cell-D60 and Cell-D120, indicating that the ZnPc molecules were considerably rearranged from an H-aggregate-dominant orientation to a mixture of H-aggregates and J-aggregates during the SAT, which can facilitate vectoral charge transport within active layers.[14,36] The broadened absorption of ZnPc between 530 nm and 850 nm post-SAT contributed to the enhanced light absorption in accordance with the enhanced J_{SC}. The polymorphic evolution of phthalocyanines by solvent treatment has been recently observed.[36-38] In these reports, the phase transformation of phthalocyanine-based donors occurred upon solvent annealing, resulting in enhanced light absorption and vectoral charge transport. Our SAT method induced a similar phase evolution, which contributed to the improvement in cell performance.

Table 2 Performance of OPVs containing ZnPc/C_{60} layers after SAT of various durations

SAT duration	V_{OC} (V)	J_{SC} (mA·cm^{-2})	FF	PCE (%)
Cell-A (0 min)	0.38	5.29	0.42	0.83
Cell-D30	0.45	5.18	0.46	1.06
Cell-D60	0.61	7.50	0.56	2.58
Cell-D90	0.40	8.61	0.41	1.41
Cell-D120	0.33	10.42	0.37	1.29

In addition to the improvement in J_{SC}, V_{OC} and FF were also significantly enhanced by post-SAT (compare Cell-A and Cell-D). In particular, V_{OC} of Cell-D (0.61 V) was higher than that of previously reported ZnPc/C_{60}-based OPVs (0.29–0.58 V).[39-44] These

results become more intriguing when the performance of Cell-B and Cell-D are compared. The J_{SC} values of both cells are similar (7.07 and 7.50 mA·cm^{-2} for Cell-B and Cell-D, respectively) because both cells have a D/A intermixed nanomorphology. However, Cell-D has significantly higher V_{OC} and FF (0.61 V and 56.4%, respectively) as compared to Cell-B (0.54 V and 38.4%, respectively). V_{OC} is related to the ratio of J_{SC} and the reverse saturation current density, J_0, based on the equivalent-circuit method [45, 46] as expressed in equation (1).

$$V_{OC} \cong n\frac{kT}{e}\ln\left(\frac{J_{SC}}{J_0}\right) \qquad (1)$$

where k is the Boltzmann constant, T is the temperature, e is the elementary charge, and n is the ideality factor. Reverse saturation current density, J_0, could be obtained by fitting the dark current J-V characteristics (Figure 2b) with a modified Schockley equation,[46,47]

$$J = J_0\left[\exp\left(\frac{e(V - JR_S)}{nkT}\right) - 1\right] \qquad (2)$$

where J is the dark current density and R_S is the cell series resistance. The J_0 values extracted were 3.5×10^{-5} mA·cm^{-2}, 2.3×10^{-5} mA·cm^{-2} and 1.1×10^{-5} mA·cm^{-2} for the Cell-A (as-prepared), Cell-B (BHJ) and Cell-D (post-SAT), respectively. The V_{OC} enhancement for the Cell-D can therefore be explained by the increased J_{SC}/J_0 values (reduced J_0 with enhanced J_{SC}), which implies the diode characteristics of the active layers were improved by the post-SAT. The FF is known to be closely to the shunt (R_P) and series resistance (R_S) of the active layers.[48] The R_P and R_S values were determined by the slopes of the characteristic J–V curves under irradiation at $V = 0$ and $J = 0$, respectively. Cell-D exhibited considerably higher R_p and lower R_s (2.8 and 0.013 kΩ·cm^2, respectively) than Cell-A (0.21 and 0.026 kΩ·cm^2) and B (0.12 and 0.021 kΩ·cm^2).

In order to further understand the origin of the superior V_{OC} and FF of Cell-D, the effect of SAT on the surface morphology of the active films was investigated using tapping-mode atomic force microscopy (AFM). As shown in Figure S5 in SI, the surfaces of the as-prepared active layers were smoother post-SAT. The root-mean-square roughness (R_{rms}) of the as-deposited films (~5.6 nm) was reduced to less than half after SAT (~2.2 nm). These facts indicate that the as-deposited films may have limited smoothness with possible internal micropores because they are formed by the sequential accumulation of thermally evaporated molecules. The reduced V_{OC} with higher J_0 in Cell-A and Cell-B as compared to Cell-D may be attributed to the leakage current through these micropores based on the fact that the higher porosity could have introduced a new resistor (R_{P2}) into the equivalent circuit, which reduced V_{OC} by a factor of $R_{P2}/(R_{P2} + R_S)$.[49]SAT can partially re-dissolve ZnPc in order to heal the micropores while smoothing the film surface. These effects can improve D/A contact, reduce the R_S, enhance the interfacial contact between the active layer and the metal electrode, and prevent metal penetration through the micropores. The spectroscopic (PL and EA) and microscopic (FE-SEM and AFM) analysis results imply that appropriate SAT of the pristine bilayers of ZnPc/C_{60} can be reorganized into void-free, smooth, dense layers by partial intermixing of ZnPc and C_{60} molecules. Based on the correlation between this nanomorphological information and J_{SC}, the resulting intermixed heterojunction structure possesses a higher interfacial area with sufficient bicontinuity, which is favorable for charge collection as compared to the conventional PHJ structure.

Conclusions

In summary, we developed a novel SAT method that can effectively manipulate the nanomorphology of ZnPc/C_{60} active layers from PHJ to BHJ-like intermixed layers. The evolution of this active layer nanomorphology could enhance all the properties for photovoltaic cells. Upon SAT of the ZnPc/C_{60} bilayer using acetone vapors, the ZnPc was re-dissolved and penetrated into the C_{60} layers while simultaneously healing the micropores within the active layers. Furthermore, the ZnPc molecules were also rearranged from H-aggregation-dominant to a mixture of H-and J-aggregation by post-SAT, which improved the light absorption properties. The nanomorphological alteration of the layers was dependent on the duration of the SAT. In terms of the benefits of the nanomorphological evolution, the post-SAT OPV (Cell-D) displayed cell performance (PCE = 2.58%) that was three times better than that of untreated bilayer cells (Cell-A, PCE = 0.83%). These results are due to the enhanced ZnPc/C_{60} interfacial area, reduced series resistance, and increased shunt resistance (reduced leakage current). Our unique SAT technique also suggests an alternative route to manipulating the nanomorphology of organic thin films by vacuum deposition, which may be very difficult to change otherwise. Applications of the SAT technique to various materials and organic thin-film electronic devices are underway in our laboratory.

Experimental

Cell fabrication: Four types of ZnPc/C_{60}-based small-molecule OPV cells were fabricated (Figure 1). The active layers had a PHJ bilayer (Cell-A), BHJ layer (Cell-B), pre-SAT bilayer (Cell-C), and a post-SAT bilayer (Cell-D). For all the samples, well-cleaned indium–tin oxide (ITO)-coated glass substrates (sheet resistance = ~10.2 Ω cm^{-2}) were first subjected to UV-ozone cleaning for 10 min. A poly(3,4-ethylenedioxythiophene):poly(styrenesulfonate) (PEDOT:PSS) solution (Clevios™ 4083, Sigma-Aldrich) was then spun on the cleaned ITO/glass substrates to form the hole-collecting (electron-blocking) buffer layers (thickness ~40 nm). The films were then dried at 100 °C for 12 h under vacuum. For Cell-A (PHJ bilayer), the active layers were grown in an ultrahigh-vacuum (UHV) organic molecular beam deposition (OMBD) chamber with a base pressure of ~2 × 10^{-8} Torr (2.67 μPa). Commercially available ZnPc powder (97%, Aldrich Chemical) was purified three times through temperature gradient sublimation. The purified ZnPc was then outgassed in the OMBD chamber for 15–20 h before growth and then sublimed from a miniature effusion cell onto the glass/ITO/PEDOT:PSS substrates held at room temperature (RT). The effusion cell temperature was 370 °C, corresponding to a growth rate of ~0.3 Å/s as determined using a quartz crystal microbalance (QCM) positioned near the substrate. The film thicknesses were also measured *ex situ* using a field-emission scanning electron microscope (FE-SEM) (JEOL JSM 740F) and atomic force microscope (AFM) (SII SPA 400). On the 350-Å-thick ZnPc layer, a 400-Å-thick C_{60} layer was deposited at a growth rate of ~0.1 Å/s (cell temperature ~390 °C) followed by a 100-Å-thick bathocuproine (BCP) layer at a growth rate of ~1.0 Å/s (cell temperature ~175 °C). C_{60} (sublimation grade, 99.9%, Sigma-Aldrich) and BCP (98.0%, Tokyo Chemical Industry) were used as received. The top electrode (Al) was then formed to a thickness of 800 Å using a thermal

evaporation technique through a shadow mask, resulting in an active area of 2 × 2 mm. Cell-B (BHJ layer) was prepared by the codeposition of ZnPc:C_{60} (1:1, thickness = 410 Å) onto the 50-Å-thick ZnPc layer previously deposited on the PEDOT:PSS/ITO. Additional C_{60} (200 Å) and BCP (100 Å) were deposited before the Al electrode (800 Å) deposition. For Cell-C (pre-SAT bilayer), the 350-Å-thick ZnPc thin film grown on the glass/ITO/PEDOT:PSS substrate was transferred to an adjacent vacuum chamber equipped with a solvent-spray system.[23] The substrate was then treated by solvent vapors for 30–120 min at RT to yield ZnPc nanopillars. The resulting films were transferred back to the OMBD chamber and dried at 100 °C for 1 h under ultrahigh vacuum. The 400-Å-thick C_{60}, 100-Å-thick BCP, and 800-Å-thick Al layers were then subsequently deposited. For Cell-D (post-SAT bilayer), the as-prepared PHJ active layer (the active layer of Cell-A) was transferred to the solvent-treating chamber. The chamber was saturated with acetone vapors obtained by the evaporation of the liquid contained in a cylinder attached to the chamber. The film was maintained under saturated acetone vapors for 30–120 min. The film was then transferred back to the OMBD chamber and dried at 100 °C for 1 h under ultrahigh vacuum. A 50-Å-thick C_{60} layer was additionally deposited, followed by the deposition of 100-Å-thick BCP and 800-Å-thick Al layers.

Characterization: The current density–voltage (J–V) characteristics of the OPV cells were measured under illumination of air mass 1.5G one sun conditions (ORIEL 91193 1000 W Xe lamp; intensity: 100 mW/cm^2) with the aid of a potentiostat (CHI 608C, CH Instrument). The surface and cross sections of the cells and individual layers were investigated using focused ion beam-scanning electron microscopy (FIB-SEM) (Nova 200, FEI Company) and atomic force microscopy (AFM). Photoluminescence (PL) spectra were recorded using a fluorescence spectrophotometer (Fluorolog-3, Horiba Jobin Yvon) with 600 nm excitation. The electronic absorption of the films was recorded using an ultraviolet-visible (UV-vis) spectrophotometer (Scinco S-3100).

Acknowledgements

The authors gratefully acknowledge support from the Basic Science Research Program, Nuclear R&D program and Nano Material Technology Development Program through the National Research Foundation of Korea (NRF, 2012045675, 2013R1A1A2A10012336, and 2011-0030233) funded by the Ministry of Education, Science and Technology, and New & Renewable Energy Core Technology Program of the Korea Institute of Energy Technology Evaluation and Planning (KETEP) granted financial resource from the Ministry of Trade, Industry & Energy, Republic of Korea (No. 20133030000210).

Notes and references

[a]*Department of Chemistry, Kookmin University, Seoul 136-702, Republic of Korea. E-mail: syjang@kookmin.ac.kr or sgyim@kookmin.ac.kr*

[b]*Korea Research Institute of Standard and Science, Daejeon 305-340, Korea*

† Electronic Supplementary Information (ESI) available: [Electronic supplementary information (ESI) available: Schematic illustration of the cell fabrication equipment, additional FE-SEM images, and AFM images]. See DOI: 10.1039/b000000x/

1 G. Salassa, J. W. Ryan, E. C. Escudero-Adan and A. W. Kleij, *Dalton Trans*, 2014, **43**, 210-221.
2 F. J. Zhang, D. W. Zhao, Z. L. Zhuo, H. Wang, Z. Xu and Y. S. Wang, *Sol Energy Mater Sol Cells*, 2010, **94**, 2416-2421.
3 T. Monch, P. Guttmann, J. Murawski, C. Elschen, M. Riede, L. Muller-Meskamp and K. Leo, *Org Electron*, 2013, **14**, 2777-2788.
4 F. Zhang, F. Sun, Y. Shi, Z. Zhuo, L. Lu, D. Zhao, Z. Xu and Y. Wang, *Energy Fuels*, 2010, **24**, 3739-3742.
5 M. A. Green, K. Emery, Y. Hishikawa, W. Warta and E. D. Dunlop, *Prog Photovoltaics*, 2011, **19**, 565-572.
6 S. R. Forrest, *Chem Rev*, 1997, **97**, 1793-1896..
7 S. Steudel, S. De Vusser, S. De Jonge, D. Janssen, S. Verlaak, J. Genoe and P. Heremans, *Appl Phys Lett*, 2004, **85**, 4400-4402.
8 D. Cheyns, K. Vasseur, C. Rolin, J. Genoe, J. Poortmans and P. Heremans, *Nanotechnology*, 2008, **19**, 424016.
9 D. H. Wang, D. G. Choi, K. J. Lee, S. H. Im, O. O. Park and J. H. Park, *Org Electron*, 2010, **11**, 1376-1380.
10 D. M. Nanditha, M. Dissanayake, A. A. D. T. Adikaari, R. J. Curry, R. A. Hatton and S. R. P. Silva, *Appl Phys Lett*, 2007, **90**, 253502.
11 P. Peumans, S. Uchida and S. R. Forrest, *Nature*, 2003, **425**, 158-162.
12 F. Yang, M. Shtein and S. R. Forrest, *Nat Mater*, 2005, **4**, 37-41.
13 F. Yang, M. Shtein and S. R. Forrest, *J Appl Phys*, 2005, **98**, 014906.
14 S. Gunes, H. Neugebauer and N. S. Sariciftci, *Chem Rev*, 2007, **107**, 1324-1338.
15 S. Sun, Z. Fan, Y. Wang and J. Haliburton, *J Mater Sci*, 2005, **40**, 1429-1443.
16 F. A. Castro, H. Benmansour, C. F. O. Graeff, F. Nuesch, E. Tutis and R. Hany, *Chem Mater*, 2006, **18**, 5504-5509.
17 M. Carrasco-Orozco, W. C. Tsoi, M. O'Neill, M. P. Aldred, P. Vlachos and S. M. Kelly, *Adv Mater*, 2006, **18**, 1754-+.
18 X. G. Liang, T. Chen, Y. S. Jung, Y. Miyamoto, G. Han, S. Cabrini, B. W. Ma and D. L. Olynick, *Acs Nano*, 2010, **4**, 2627-2634.
19 N. Li and S. R. Forrest, *Appl Phys Lett*, 2009, **95**.
20 J. G. Van Dijken, M. D. Fleischauer and M. J. Brett, *J Mater Chem*, 2011, **21**, 1013-1019.
21 J. G. Van Dijken, M. D. Fleischauer and M. J. Brett, *Org Electron*, 2011, **12**, 2111-2119.
22 H. X. Xi, Z. M. Wei, Z. M. Duan, W. Xu and D. B. Zhu, *J Phys Chem C*, 2008, **112**, 19934-19938.
23 J. Kim, C. R. Park and S. Yim, *RSC Advances*, 2012, **2**, 963-967.
24 J. Kim and S. Yim, *Materials Research Bulletin*, 2012, **47**, 2744-2747.
25 P. Heremans, D. Cheyns and B. P. Rand, *Accounts Chem Res*, 2009, **42**, 1740-1747.
26 S. Banerjee, A. P. Parhi, S. S. K. Iyer and S. Kumar, *Appl Phys Lett*, 2009, **94**.
27 Q. L. Song, F. Y. Li, H. Yang, H. R. Wu, X. Z. Wang, W. Zhou, J. M. Zhao, X. M. Ding, C. H. Huang and X. Y. Hou, *Chem Phys Lett*, 2005, **416**, 42-46.
28 J. J. Steele and M. J. Brett, *J Mater Sci-Mater El*, 2007, **18**, 367-379.
29 K. H. Lee, P. E. Schwenn, A. R. G. Smith, H. Cavaye, P. E. Shaw, M. James, K. B. Krueger, I. R. Gentle, P. Meredith and P. L. Burn, *Adv Mater*, 2011, **23**, 766-+.
30 A. L. Ayzner, C. J. Tassone, S. H. Tolbert and B. J. Schwartz, *J Phys Chem C*, 2009, **113**, 20050-20060.

31 H. Y. Park, K. Kim, D. Y. Kim, S. K. Choi, S. M. Jo and S. Y. Jang, *J Mater Chem*, 2011, **21**, 4457-4464.
32 J.-S. Kim, W.-S. Chung, K. Kim, D. Y. Kim, K.-J. Paeng, S. M. Jo and S.-Y. Jang, *Adv Funct Mater*, 2010, **20**, 3538-3546.
33 M. Szybowicz, T. Runka, M. Drozdowski, W. Bala, M. Wojdyla, A. Grodzicki, P. Piszczek and A. Bratkowski, *J Mol Struct*, 2007, **830**, 14-20.
34 H. Gong, J. Kim and S. Yim, *B Korean Chem Soc*, 2012, **33**, 825-827.
35 Y. F. Qiu, P. L. Chen and M. H. Liu, *Langmuir*, 2008, **24**, 7200-7207.
36 D. Placencia, W. N. Wang, J. Gantz, J. L. Jenkins and N. R. Armstrong, *J Phys Chem C*, 2011, **115**, 18873-18884.
37 D. Placencia, W. N. Wang, R. C. Shallcross, K. W. Nebesny, M. Brumbach and N. R. Armstrong, *Adv Funct Mater*, 2009, **19**, 1913-1921.
38 W. N. Wang, D. Placencia and N. R. Armstrong, *Org Electron*, 2011, **12**, 383-393.
39 Y. Terao, H. Sasabe and C. Adachi, *Appl Phys Lett*, 2007, **90**, 103515.
40 W. J. Zeng, K. S. Yong, Z. M. Kam, F. R. Zhu and Y. N. Li, *Appl Phys Lett*, 2010, **97**, 133304.
41 B. Yu, L. Z. Huang, H. B. Wang and D. H. Yan, *Adv Mater*, 2010, **22**, 1017-1020.
42 S. Pfuetzner, C. Mickel, J. Jankowski, M. Hein, J. Meiss, C. Schuenemann, C. Elschner, A. A. Levin, B. Rellinghaus, K. Leo and M. Riede, *Org Electron*, 2011, **12**, 435-441.
43 S. Schafer, A. Petersen, T. A. Wagner, R. Kniprath, D. Lingenfelser, A. Zen, T. Kirchartz, B. Zimmermann, U. Wurfel, X. J. Feng and T. Mayer, *Phys Rev B*, 2011, **83**, 165311.
44 W. Tress, K. Leo and M. Riede, *Sol Energy Mater Sol Cells*, 2011, **95**, 2981-2986.
45 W. J. Potscavage, A. Sharma and B. Kippelen, *Accounts Chem Res*, 2009, **42**, 1758-1767.
46 M. D. Perez, C. Borek, S. R. Forrest and M. E. Thompson, *J Am Chem Soc*, 2009, **131**, 9281-9286.
47 P. Yang, M. Yuan, D. F. Zeigler, S. E. Watkins, J. A. Lee and C. K. Luscombe, *J Mater Chem C*, 2014, **2**, 3278-3284.
48 B. P. Rand, J. Genoe, P. Heremans and J. Poortmans, *Prog Photovoltaics*, 2007, **15**, 659-676.
49 A. Moliton and J. M. Nunzi, *Polym Int*, 2006, **55**, 583-600.